A multi-fluid model of the magnetopause

Roberto Manuzzo[1,2], Francesco Califano[2], Gerard Belmont[1], and Laurence Rezeau[1]

[1]LPP, CNRS, Ecole Polytechnique, Sorbonne Université, Univ. Paris-Sud, Observatoire de Paris, Université Paris-Saclay, PSL Research University
[2]Department of Physics E. Fermi, Universitá di Pisa, Italia

Correspondence: F. Califano (francesco.califano@unipi.it)

Abstract. Observation of the solar wind - magnetosphere boundary provides a unique opportunity to investigate the physics underlying the interaction between two collisionless magnetized plasmas with different temperature, density and magnetic field topology. Their mixing across the interface as well as the boundary dynamics are affected by the development of fluid (and kinetic) instabilities driven by large scale inhomogeneities in particle and electromagnetic fields. Building up a realistic initial equilibrium state of the magnetopause according to observations is still a challenge nowadays. In this paper we address the modeling of the particles and electromagnetic fields configuration across the Earth's magnetopause by means of a three-fluid analytic model. The model relies on one hot and one cold ion population and on a neutralizing electron population. The goal is to build up an analytic model able to reproduce as closely as possible the observations. Some parameters of the model are set by using a fit procedure aiming at minimizing their difference with respect to experimental data provided by the Magnetospheric MultiScale mission. All the other profiles, concerning the electron pressure and the relative densities of the cold and hot ion populations, are calculated in order to satisfy the fluid equilibrium equations. Finally, by means of a new tri-fluid code, we have checked the stability of the large-scale equilibrium model for a given experimental case and given the proof that the system is unstable to reconnection. This model could be of interest for the interpretation of satellite results and for the study of the dynamics at the boundary between the magnetosphere and the solar wind.

1 Introduction

The solar wind - magnetosphere boundary, known as the magnetopause, is characterized by the presence of magnetic and velocity shears as well as jumps in magnetic and velocity magnitudes, and in plasma density and temperature. These inhomogeneities are the sources of many plasma instabilities at different spatio-temporal scales (Labelle and Treumann, 1988), in turn often triggering themselves secondary instabilities at smaller scales. As an example, secondary instabilities such as magnetic reconnection, Kelvin-Helmholtz and/or Rayleigh-Taylor instability can efficiently develop on the shoulder of the primary instability as for instance the Kelvin-Helmholtz instability at the low latitude magnetopause (see Faganello and Califano (2017) and references therein).

All of these phenomena can cause significant entry of magnetosheath plasma mass (Paschmann, 1997), momentum (Dungey, 1961) and energy (Lee and Roederer, 1982) into the magnetosphere. The study of the magnetopause is of particular interest since this system offers the unique opportunity to study a two-plasma large-scale interaction in conditions not achievable in laboratory. The magnetopause physics is also of basic importance in the studies addressing the Sun-Earth interaction, in particular concerning the impact of solar wind disturbances on the terrestrial environment and the attempts of space-weather forecasting (see for instance Baker and Lanzerotti (2016)). The question of modelling space plasmas using data provided by multi-spacecraft missions has been much developed during (and in preparation of) the Cluster era (Büchner et al., 1998). Concerning the magnetopause data, one of the key points concerns the mixing between magnetospheric and magnetosheath plasmas and the resulting non-Maxwellian shape of the distribution functions (hereafter d.f.) observed in these regions (Bosqued et al. (2001), Frey et al. (2003), Phan et al. (2005), Retinò et al. (2005)). These d.f. are often reminiscent of those observed in reconnection kinetic simulations (Nakamura and Scholer (2000), Tanaka et al. (2008), Aunai et al. (2011)). Some of these d.f. can be compared with simple analytic models as in the pioneering work by Cowley and Owen (1989). Since the populations coming from the two different sides of the magnetopause differ in density and in temperature, modeling the mixing requires at least the use of a multi-population model. In the perspective of investigating the dynamics of the magnetopause mixing layer by a three-fluid numerical simulation, the main target of this paper is to build up a three-fluid equilibrium as realistic as possible for initializing it.

The three-fluid model that we propose in the present paper aims at distinguishing between the ions of magnetospheric and magnetosheath origins. It must be considered as a first step towards a four-population model, which would also allow distinguishing the electrons of both origins. This simplification allows to avoid the non essential details related to the presence of two electron species, which are likely not to have a major role for structuring the large-scale equilibrium. In addition, note that for a correct modeling of the electrons in the magnetopause vicinity, one should also split the magnetospheric electrons into at least two sub-populations, one "cold" poorly measured, carrying the density, and one "hot", carrying the pressure. Finally, starting from a previously existing two-fluid code, it is relatively straightforward to build up a multi-ion one-electron code where the electrons just provide an "Ohm's law". On the contrary a fully multi-population code (*i.e.* including several electron populations) requires a radically different approach presently under investigation and matter for future work.

In the past, several multi-population models trying to simulate the plasma interaction between magnetosheath and magnetosphere have been developed. In particular, for the modeling of tangential layers (*i.e.* without normal magnetic field and without normal velocity, $B_n = u_n = 0$), the kinetic models are by definition the most complete ones since they rely on a Vlasov equilibrium. Nevertheless, since these models are considerably more complicated than the fluid ones, using the latter can be considered as a necessary first step for the purpose of modeling the magnetopause as close as possible to the observational data. Note also that all the equilibria built via distribution functions that are only single-valued functions of the particle invariants of motion (Channell (1976)) cannot really be considered as "multi-population" models: they ignore the questions of accessibility (Whipple et al. (1984)) and therefore they cannot distinguish between particles of magnetospheric or magnetosheath origins. Some models (Roth et al. (1996), De Keyser and Roth (1998)) have partly accounted for the accessibility problem by considering functions of the invariants that are bi-valued. In these last years new models have been developed by

Belmont et al. (2012) and Dorville et al. (2015) to take it into account by considering more general multi-valued distribution functions. Nevertheless, it must be kept in mind that all these models involve many free parameters. In Dorville et al. (2015), the authors even emphasize that there is no general constraint for fixing the normal electric field profile in their kinetic model, in which this one can be chosen fully arbitrarily. On the top of that, even if a few profiles can be fixed in a more or less realistic way, all the others depend on simple mathematical assumptions, which are largely arbitrary, so that they generally still remain far from realistic.

A different approach to build up a large scale configuration at the boundary between the magnetosheath and the magnetosphere is to run a global simulation eventually reaching a steady state. This has been done recently via hybrid and kinetic codes (Chen et al. (2017), Palmroth et al. (2018)), even if the question of spatial resolution is then difficult to solve for investigating the internal structure of the magnetopause boundary. It will be interesting to compare the results obtained by these methods with those obtained by the methods discussed in the present paper where the model relies instead on spacecraft data as initial condition for the simulation.

In summary, the lack of realistic equilibria in the literature generally makes difficult, for kinetic simulations, the initialization of the magnetopause studies. Recently the multi-population character of the medium has been taken into account in a recent paper (Dargent et al., 2017) for a different goal. Using a PIC code, they investigate the influence of cold magnetospheric ions on the development of magnetic reconnection. In this paper, the magnetospheric plasma includes two populations with different temperatures in order to account for the presence of the cold ions that are observed in the magnetosphere close to the magnetopause.

Multi-fluid models have been developed in various domains, but in general not for magnetopause studies. These studies address multi-species evolution involving chemical processes and collisions. They have been used to investigate planetary atmospheres (Modolo et al. (2006), Ma et al. (2007)), the solar chromosphere (Alvarez Laguna et al., 2016), and basic plasma physics problems (drift turbulence in Shumlak et al. (2011) for instance).

In this paper we present a new technique to build up a three fluid equilibrium that derives directly from satellite observations. The model assumes uni-dimensional gradients in the normal direction and a tangential boundary ($B_n = 0$) at the magnetopause. The magnetic and velocity shear are both taken into account in a realistic way. The profiles are chosen to fit at best data from the Magnetospheric MultiScale mission (MMS) (Burch et al., 2016b) for which the time-to-space conversion has been performed by means of recent techniques presented in (Manuzzo et al., 2019). As it will be shown in section (4), the method provides a cold and a hot contributions in qualitative agreement with observations, even if the model uses, as inputs, only the global ion macroscopic moments.

2 Observations

We use MMS data during the period October 16th 2015, 13:05:34 + 40s UT, occurred at $[8.3, 8.5, -0.7]R_E$ in GSE frame, which embeds a magnetopause crossing. In Figure (1) we plot the experimental data that the equilibrium model attempts to
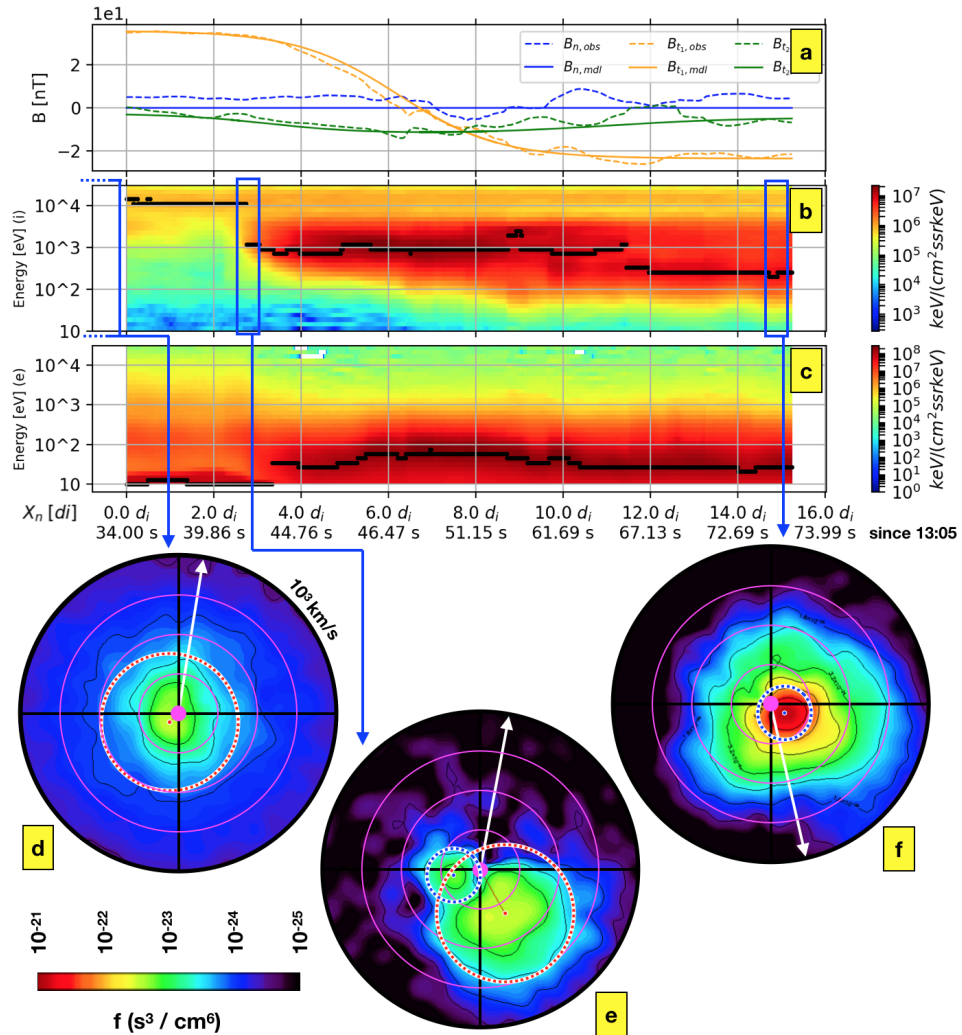
Figure 1. MMS data for the October 16th 2015, 13:05:34 UT + 40s event. Panel a: normal and tangential (to the magnetopause plane) components of the magnetic field. Panels b and c: ion and electron spectrograms. The first abscissa is the spatial coordinate normal to the magnetopause X_n (see text) and the second one is time. Panels d, e and f: ion distribution functions recorded by the FPI instruments, respectively in the magnetosphere, in the overlapping region and in the magnetosheath. These i.d.f.s are projected on the tangential plane by integration over the normal component of the velocity.

reproduce. This interval shows the standard signatures of the region where magnetospheric and magnetosheath plasmas meet (magnetopause crossing): reversal of the magnetic field and change in the energy distributions.

In panels (a), (b) and (c) data are plotted as functions of a spatial coordinate X_n, which is the projection of the spacecraft path along the direction normal to the magnetopause (units of $d_{i,MSh}$ with $d_{i,MSh} \simeq 70$ km). Once the function $X_n(t)$ is known, it allows to recover the spatial profiles of all quantities of interest from the corresponding temporal series of the spacecraft magnetosheath - magnetosphere crossing, even with a variable velocity. For the sake of completeness, we give also in the abscissa of panel (c) the time corresponding to each given value of X_n. The spatial coordinate $\mathbf{X}(t)$ is determined by integration of the velocity of the spacecraft with respect to the magnetic structure. In order to determine this spatial velocity, we use here a new method (Manuzzo et al., 2019), which is an extension of the STD method first proposed by (Shi et al., 2006). The main difference with respect to the Shi model consists in taking into account the possible weak non-stationarities of the magnetic structure, *i.e.* assuming $\partial_{t,sc}\mathbf{B} = \partial_{t,0}\mathbf{X} \cdot \nabla \mathbf{B} + \partial_{t,0}\mathbf{B}$ and not just $\partial_{t,sc}\mathbf{B} = \partial_{t,0}\mathbf{X} \cdot \nabla \mathbf{B}$ (the indexes "*sc*" and "0" indicate the spacecraft frame and the frame where the intrinsic variation of the magnetopause structure are the smallest, respectively). This allows to avoid some singularities in the results.

In the two spectrograms (panels b and c), black points have been over-plotted to indicate their maxima. This allows one to individuate more easily where the magnetosheath and the magnetospheric plasma interact, as indicated by discontinuities in the curve joining the maxima. The region where the two plasmas partially overlap in space is emphasised by a blue rectangle in panel (b), centred at $X_n \sim 3\ d_i$.

In panels (d), (e) and (f) we plot the 2D ion distribution functions (i.d.f.) in the plane tangential to the magnetopause. They are obtained by integration over the out-of-plane (normal) component of the velocity. Each plot is the average of 5 single i.d.f recorded within a $\sim 0.75s$ long interval (equivalent to $0.5d_i$). The radius of the distribution functions is 10^3 km/s and the purple full circle drawn at their centres determines the bottom limits in energy of the FPI instrument (10 eV ~ 53 km/s for ions). The direction of the local magnetic field is indicated by a white arrow. In panel (e) (mixing region), one can observe that the i.d.f. contains two peaks emphasised by the over-plotted circles (blue and red dashed lines). These two circles have a diameter equal to the magnetosheath and magnetospheric thermal velocities, respectively. The same circles are shown for the magnetosheath and magnetospheric i.d.f.s, (f) and (d) panels. In these two asymptotic media, we see that there is only one single peak. Note that the i.d.f. shown in panel (d) has been recorded a little earlier (10:20:00 UT + 2s) during a "clear" observation of the magnetosphere allowing to avoid the presence of magnetosheath particles when the spacecraft is too close to the magnetopause. On the other hand panel (e) shows a mixture of the magnetosheath and magnetospheric populations at the same time. However, since the two peaks are close to each other and since the distributions of the two populations are partly superposed, it is not possible to clearly separate the hot/cold contributions, a necessary input for the multi-population model to be built by a direct fit of this region. We will explain in the next section a new method capable of separating the two particle components even in such complex situations. Note that, in the magnetospheric region ($X_n \leq 2d_i$) the electron spectrogram of panel (c) shows energy maxima that lay just at the bottom limit of the instrument ($\simeq 10\ eV$). This indicates the presence of cold electrons in the magnetosphere. The role of this poorly measured cold electron population is not relevant for the magnetopause pressure equilibrium, but in the electron bulk velocity it could be significant. However the electron population parameters will

be not determined by a direct fit of the data, nor will those of the two ion populations (cold/hot). They will be determined instead by another method based on the equilibrium equations, which we will describe in the next section.

3 The three fluid model

3.1 Equilibrium equations

We present here a 3fluid collisionless model which includes two proton populations (one cold and one hot) and one electron population. The cold ion population models the ions of magnetosheath origin and disappears more and more on the magnetospheric side. Conversely, the hot population models the ions of magnetosphere origin and disappears on the magnetosheath side.

The continuity and ion momentum equations are derived from the first two moments of the Vlasov equation. We impose charge neutrality and the displacement current is neglected. We assume isotropic pressures and adopt a polytropic closure for all populations. These equations are coupled to the electromagnetic field via the Faraday's equation and we use an Ohm's law taking into account the electron pressure gradient but neglecting electron inertia effects. The 3fluid system of equations reads:

$$
\begin{cases}
\sum_{\alpha} n_\alpha q_\alpha = 0 & \text{(1a)} \\[2mm]
\sum_{\alpha} n_\alpha q_\alpha \mathbf{U}_\alpha = \nabla \times \mathbf{B}/\mu_0 & \text{(1b)} \\[2mm]
\dfrac{\partial n_\beta}{\partial t} + \nabla \cdot (n_\beta \mathbf{U}_\beta) = 0 & \text{(1c)} \\[2mm]
\dfrac{\partial (n_\beta m_\beta \mathbf{U}_\beta)}{\partial t} + \nabla \cdot (n_\beta m_\beta \mathbf{U}_\beta \mathbf{U}_\beta) + \nabla (n_\beta T_\beta) = n_\beta q_\beta \left(\mathbf{E} + \mathbf{U}_\beta \times \mathbf{B}\right) & \text{(1d)} \\[2mm]
\dfrac{\partial (n_\alpha S_\alpha)}{\partial t} + \nabla \cdot \left[\mathbf{U}_\alpha (n_\alpha S_\alpha)\right] = 0 \ ; \ S_\alpha = T_\alpha n_\alpha^{1-\gamma} & \text{(1e)} \\[2mm]
\dfrac{\partial \mathbf{B}}{\partial t} = -\nabla \times \mathbf{E} & \text{(1f)} \\[2mm]
\mathbf{E} = -\mathbf{U}_e \times \mathbf{B} + \dfrac{1}{n_e q_e} \nabla (n_e T_e) & \text{(1g)}
\end{cases}
$$

Here the index α stands for "all populations" and the index β for "all ion populations".

3.2 Determination of the fluid profiles

We aim at establishing a tangential 1D equilibrium to mimic as close as possible the magnetopause observations previously presented. Assuming $\partial/\partial t = 0$, this is done in three steps.
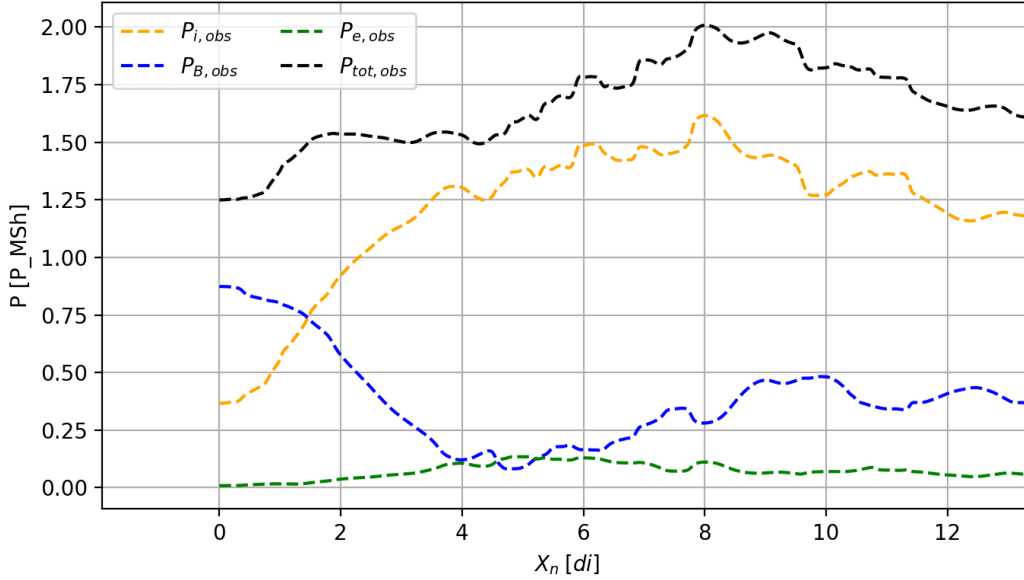
Figure 2. Comparison between P_e, P_i, P_B. The total pressure is indicated as P_{tot}. Numerical values are all normalized to the magnetosheath pressure $P_{MSh} \sim 3200$ eV cm^{-3}.

Step 1: We impose the magnetic field $\mathbf{B}$, the density n_i, temperature T_i and velocity $\mathbf{U}_i$ profiles by fitting the data using a combination of hyperbolic tangents as explained in section (4). At this stage the ion quantities are chosen without distinguishing the cold and hot populations.

Step 2: We deduce the electron density n_e and velocity $\mathbf{U}_e$ by using the equilibrium equations (1a) and (1b). The temperature T_e is deduced from

$$P_e = P_{tot} - (P_B + n_i T_i) \tag{2}$$

where the total pressure, P_{tot}, has been imposed to be constant in order to fulfil the equilibrium conditions.

As far as P_e is concerned, we note that i) P_e is much smaller than $P_i + P_B$ (see Fig. 2) and that ii) it is difficult to estimate it precisely because of experimental uncertainties. As a consequence, the constant value of P_{tot} used in the model is taken as the maximum of the measured total pressure $P_i + P_B + P_e$. Note that the total pressure is not really constant because of the mentioned uncertainties on P_e and because the experimental structure may be slightly out of equilibrium. The modeled P_e is deduced from equation 2, the choice for P_{tot} ensuring only positive values for P_e. Finally, the electric field $\mathbf{E}$ is deduced from the Ohm's Law, Equation (1g).

Step 3: We now split the global proton population into two different populations, cold and hot (hereafter "ic" and "ih", respectively) to distinguish the magnetospheric and magnetosheath populations. The densities (n_{ic} and n_{ih}), pressures (P_{ic} and P_{ih}) and currents ($\mathbf{J}_{ic}$ and $\mathbf{J}_{ih}$) of the two ion populations add to form the total ion density, pressure and current as follows

$$n_i = n_{ic} + n_{ih} \tag{3a}$$

$$n_i T_i = n_{ic} T_{ic} + n_{ih} T_{ih} \tag{3b}$$

$$n_i \mathbf{U}_i = n_{ic} \mathbf{U}_{ic} + n_{ih} \mathbf{U}_{ih} \tag{3c}$$

The temperatures of the cold and hot ion populations, T_{ic} and T_{ih}, are assumed to be constant. Since the global ion temperature profile T_i is known, their values are obtained from the satellite data by the two limits:

$$\lim_{x \to MSph} T_{ih} = T_i \,; \quad \lim_{x \to MSh} T_{ic} = T_i$$

The temperature ratio between the two populations is set by the value of the dimensionless parameter:

$$\Upsilon \equiv \frac{T_{ih}}{T_{ic}} \tag{4}$$

Using Equation (3b), the contributions of each population to density and pressure are fully determined by the T_i profile and the temperature ratio Υ:

$$\Gamma \equiv \frac{n_{ic}}{n_i} = \frac{\Upsilon - \frac{T_i}{T_{ic}}}{\Upsilon - 1} \tag{5a}$$

$$\Pi \equiv \frac{P_{ic}}{P_i} = \left(1 + \frac{1 - \Gamma}{\Gamma} \Upsilon\right)^{-1} \tag{5b}$$

The perpendicular currents and by consequence the corresponding velocities, are fully determined by Equations (1d). On the contrary, the parallel currents cannot be determined by the above system of equilibrium equations. We will set them by a reasonable choice for the parameter ϕ which is equal to the ratio of the cold parallel ion current to the total parallel ion current as seen in the electron frame:

$$\phi \equiv \Gamma \frac{(\mathbf{U}_{ic} - \mathbf{U}_e) \cdot \mathbf{b}}{(\mathbf{U}_i - \mathbf{U}_e) \cdot \mathbf{b}} \tag{6}$$

The parallel components of the hot and cold ion velocities can have opposite directions, so that ϕ is defined in the $[-1, 1]$ range, while Γ and Π are defined in the $[0, 1]$ range. The reasonable choice for ϕ is suggested by the data and will be discussed in more details in the next section. In general, the asymptotic values of the cold and hot ion currents are chosen in agreement with the asymptotic values of n_{ic} and n_{ih}, in order that all the corresponding values of the velocities U_{ic} and U_{ih} have reasonable values, although one of the two densities n_{ic} or n_{ih} tends to nearly zero on each side.

In order to implement this model into a numerical simulation, a compromise is necessary since the multi-fluid code cannot deal with a population having a zero density somewhere in the domain. To avoid this problem, we introduce the parameters $\epsilon^{(c)} \ll 1$ and $\epsilon^{(h)} \ll 1$ and we modify the initialisation so that the cold and hot densities tend to $\epsilon^{(h)} n_i$ and $\left(1 - \epsilon^{(h)}\right) n_i$ on the magnetospheric side, and vice versa to $\left(1 - \epsilon^{(c)}\right) n_i$ and $\epsilon^{(c)} n_i$ on the magnetosheath side. The temperatures are changed

according to:

$$T_{ic} = \frac{\epsilon^{(c)} T_i^{MSph} - \left(1 - \epsilon^{(h)}\right) T_i^{MSh}}{\epsilon^{(c)} + \epsilon^{(h)} - 1} \tag{7a}$$

$$T_{ih} = \frac{\epsilon^{(h)} T_i^{MSh} - \left(1 - \epsilon^{(c)}\right) T_i^{MSph}}{\epsilon^{(c)} + \epsilon^{(h)} - 1} \tag{7b}$$

where T_{ic} and T_{ih} indicate the observed values corresponding to the model, and T_i^{MSph} and T_i^{MSh} the temperatures corre-
190 sponding to the magnetospheric and magnetosheath values of T_i. A similar correction is made for the ion velocities (see next
sections).

4 Data vs analytic profiles

We apply the procedure to the case study introduced in section (2). In Figure (3) we compare the model field profiles with the
ones obtained with the MMS data. The model profiles for the magnetic field, the ion temperature and density are obtained by a
195 fit procedure, panels (a), (b), and (c), respectively, while the others are calculated from the equilibrium equations. The fits are
obtained by means of analytic functions. For a given quantity Q, the fitting functions have the following form:

$$Q = \sum_j a_{Q,j} + b_{Q,j} tanh(\frac{X_n - c_{Q,j}}{d_{Q,j}}) \tag{8}$$

where X_n is the coordinate along the direction normal to the magnetopause (as discussed in section 2). The parameters $a_{Q,j}$,
$b_{Q,j}$, $c_{Q,j}$, and $d_{Q,j}$ are the free parameters shaping the analytic profiles and j is the component index. The maximum value
200 of j depends on the fitted quantity: the analytic profiles are considered as good fits of the data if they correctly shape the large
scale configuration, as well as the position and the length scale of the gradients within the magnetopause layer. An example of
such a "good fit" is given in Fig. 3, panels (a), (b) and (c). It is worth noticing that the particle boundary, observed on density
and temperature, has a length scale smaller than the magnetic boundary (by a ratio $\simeq 0.25$) and that its position is considerably
shifted toward the magnetosphere with respect to the centre of the magnetic jump. This may indicate the presence of a boundary
205 layer, possibly made of magnetosheath plasma observed on the magnetospheric side of the magnetopause (Hasegawa, 2012).
Such features cannot be reproduced in the framework of a MHD equilibrium model. To the best of our knowledge, they have
not been introduced even in the context of a kinetic model.

In panel (b) we show the temperature profiles as obtained with our model equilibrium. The total ion population temperature
T_i has been obtained by fit, and it is superposed with the cold ion population temperature T_{ic} (blue curve) and the hot ion
210 population one T_{ih} (red curve). The figure has been drawn using $\epsilon^{(h)} = 0.35$ and $\epsilon^{(c)} = 0.05$, which determines the values of
T_{ic} and T_{ih} via Eqs.(7).

One observes that the global temperature is well fitted by the model outside the mixing region, but that the fit is less
accurate in the $\sim 1.0 d_i \leq X_n \leq \sim 2.5 d_i$ interval. In this interval the real total ion temperature becomes actually larger than its
magnetospheric asymptotic limit. Unfortunately this feature can not be reproduced by the present 3fluid model with hot and
215 cold constant temperatures since the $\Gamma \geq 0$ constraint forces the T_i profile to be everywhere lower than T_{ih} (see Equation (5a)).

This little deviation is acceptable since the model mainly aims at reproducing the asymptotic trends, the observed inner region probably being out of equilibrium.

In panel (c) we show the density profiles. As explained in the previous section, the hot and cold ion contribution to the total density n_i are computed by means of the Γ function which is fixed once the global T_i profile and the temperature ratio Υ are fixed (Equation (5a)). For all panels of Figure (3) the two vertical lines (dashed black) indicate the limits of the region where $1/4 \leq \Gamma \leq 3/4$. Note that the cold ion density falls rapidly to very low values in more or less $\sim 2\, d_i$ (where $d_i \simeq 70$ km is the ions inertial length measured in the magnetosheath) while the hot population density keeps nearly the same value over a longer interval (between 0 and 8 d_i).

The electron density and velocity profiles are obtained from the equilibrium equations. However these quantities are not plotted here since their experimental counterparts are likely to be biased in the magnetosphere by the cold electron population which is below the bottom threshold in energy of the FPI instrument (as mentioned in section 2). On the other hand, we plot in panel (d) the normal component of the electric field, which is obtained from the 3fluid model, Equation (1g). We see that the electric field calculated by the model agrees quite well with the experimental one. Since the electric field reflects the electron dynamics this shows, independently from the electron measurements, that the electron dynamics is correctly accounted in the model.

The parallel components of the cold and hot ion currents are set by ϕ (Equation 6). As long as there are no cold ions on the magnetospheric side and no hot ions on the magnetosheath side, the asymptotic constraints on ϕ would be

$$\lim_{x \to MSph} \phi = 0\,; \quad \lim_{x \to MSh} \phi = 1$$

Nevertheless, because of the compromise necessary for implementing the model in the multi-population numerical simulation, the cold and hot densities actually take small but not strictly null values on both sides. To determine the corresponding parallel currents, corrections similar to Eqs. (7) are applied with the assumption that, on each side, the parallel velocities of the cold and hot populations, in the electron frame, are equal to each other and therefore equal to the global one. Under this assumption, it can be easily shown that the asymptotic values of Φ are equal to those of Γ:

$$\lim_{x \to MSph} \phi = \epsilon^{(h)}\,; \quad \lim_{x \to MSh} \phi = 1 - \epsilon^{(c)},$$

Note that for the particular MMS event considered, the global ion parallel velocities are observed to be quasi-null on each side, so that the same asymptotic property holds for the velocities of the two populations.

Between the two limits above, a reasonable choice for the ϕ profile is that the length of its gradients be of the same order as the scale length of the density and temperature gradients, $i.e. \sim 1 - 2\, d_i$. The position of the main gradient of ϕ is set in order to separate the magnetopause thickness in two parts, each of length proportional to the gyro-radii of the two populations (their ratio is $\simeq 2$).

In panel (e) of Figure (3) we show the model profiles for Γ, Π and Φ. Because of the differences of temperature between the two components, the profile in Π (concerning the pressures) noticeably differs from the profile in Γ (concerning the densities).

Finally, in panels (f) and (g) of Figure (3), we show the results concerning the parallel and perpendicular components of the ion currents. Once more, one observes that the global ion current is well fitted, at the exception of the perpendicular current in
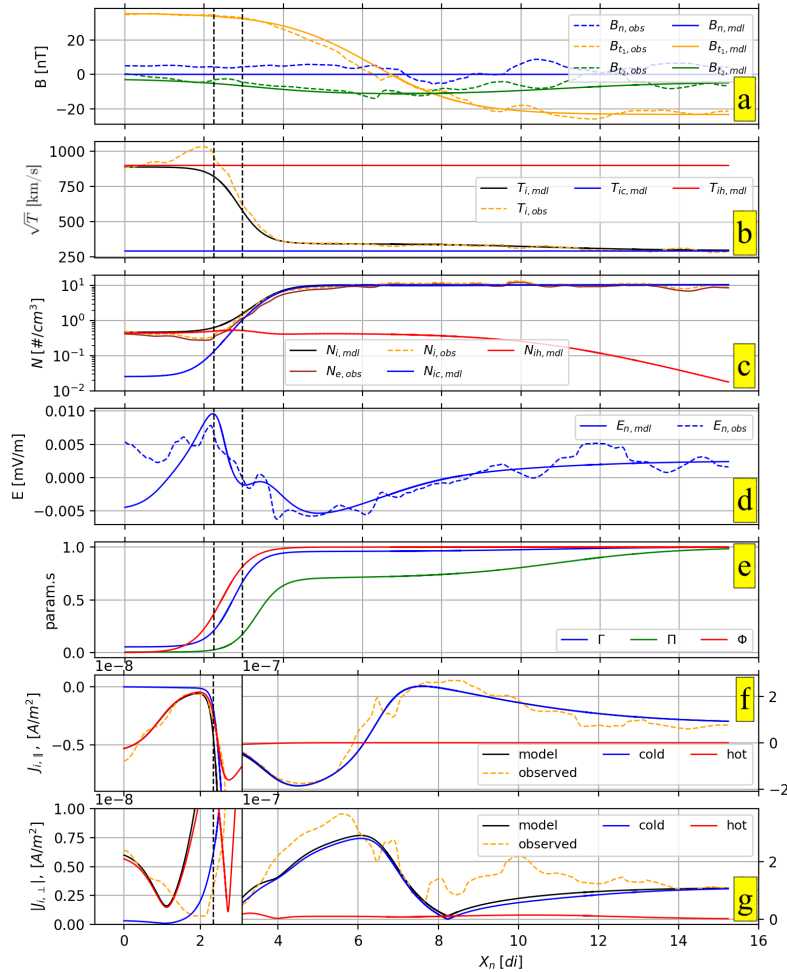
Figure 3. Comparison between the magnetopause profiles as observed by MMS during the 16 October 2015, 13:05:34 + 40s UT period and those used for the 3fluid model equilibrium. Satellite data are represented by dashed lines, the extrapolated profiles used in the model by continuous lines. The X_n coordinate represents the spatial coordinate normal to the magnetopause X_n. In the panels we show the magnetic field (a), the temperatures (b), the density (c), the normal component of the electric field (d), the parameter Γ, Π and Φ (e), and the parallel and perpendicular components of the ion current (panels f and g respectively) as computed from particle data. The two vertical lines (black dashed) highlight the transition region ($1/4 \leq \Gamma \leq 3.4$). The blue and orange colours adopted for the electric and magnetic fields represent the normal and the tangential components of the fields. The square roots of the temperatures (panel b) are plotted in velocity units in order to make easier the comparison with i.d.f.s shown in Figure (1). For the sake of clarity, the curves shown in panels (f) and (g) have been multiplied by a factor 10 in the $0.0 \leq X_n \leq 3.0$ interval.

250   the mixing region, which is less accurate. This is due to the small inaccuracy already mentioned of the modeled ion temperature in this region.

5   Numerical simulations

5.1   Set up

Here we give an example of a 3fluid numerical simulation aiming at demonstrating the possibility of studying numerically the
255   above system starting from an equilibrium not far from a real one, not only qualitatively but also quantitatively. For the sake of simplicity we limit here to a 2D geometry, the numerical code being fully 3D. A detailed numerical study relying on such approach will be the focus of future work.

The three-fluid model introduced in this paper has been used to initialize a 2D 3fluid numerical simulation of the interaction between the solar wind and the Earth's magnetopause. The numerical simulation is intended to mimic the October 16th 2015,
260   13:05:34 + 40s UT MMS crossing. This simulation has been performed by using a 3fluid numerical code that solves the set of Equations (1a-g). The code originates from a 2fluid 3D parallel code largely used for the study of the interaction of the solar wind with the magnetosphere (see Fadanelli et al. (2018) and references therein). The 3fluid code adapts the new equations to the algorithm of the 2fluid code presented in Faganello et al. (2009). It advances in time with a standard third-order Runge-Kutta algorithm (Canuto, 1988). It uses sixth order explicit finite differences along the periodic y-direction and a sixth-order
265   compact finite difference scheme with spectral like resolution for spatial derivative along the inhomogeneous x-direction (see Ref. Lele (1992) for the significance and technical details of compact finite differences with spectral like resolution). The numerical stability is guaranteed by means of a spectral filter along the periodic y-direction and a spectral-like filtering scheme along the inhomogeneous x-direction. The code is parallelized along the periodic y-direction (Lele, 1992). The code has been validated by standard numerical tests. In particular, by selecting separately the two cold and hot ion populations, we have
270   reproduced the propagation of ion acoustic and Alfvén waves.

To initialize the simulation presented in this paper we take as initial equilibrium the model profiles represented in Figure (3), including the few modifications for the cold and hot ion density components (with respect to the basic model) because of the computational reasons discussed at the end of Section 3. The three-fluid code handles a normalised version of the three-fluid set of equations (1) using the following characteristic quantities. Magnetic field and ion densities are normalized to their
275   mean values in the magnetosheath (out of the magnetopause layer) $B_0 = B_{MSh}$ and $n_0 = n_{MSh}$. Velocity is normalized to the corresponding Alfvén velocity $V_0 = V_{A,MSth} = B_0/\sqrt{(\mu_0 n_0 m_i)}$ and time to the corresponding inverse ion gyro-frequency $t_0 = 1/\Omega_{c,MSh} = m_i/q_i B_0$. The other normalization quantities are obtained from those just introduced: the lengths to $l_0 = V_0 t_0$ (i.e. the ion inertial length), the temperatures to $T_0 = m_i V_0^2$ and the electric field to $E_0 = V_0 B_0$.

The simulation box dimensions are given by $L_x = 160 \; d_i$, $L_y = 20\pi \; d_i$ and the box is discretized using $n_x = 800$ and
280    $n_y = 320$ grid points corresponding to $dx = dy = 0.2 \; d_i$. We have checked that the equilibrium configuration remains stable for several thousands of ion cyclotron times in the absence of an initial perturbation because of the very low values of the numerical noise and of the high accuracy of the numerical method.

5.2 Results

The large scale equilibrium configuration used to initialize the simulation is unstable with respect to the reconnection mode. At $t = 0$ we add to the equilibrium an initial perturbation $\delta \mathbf{B} = \nabla \times \mathbf{A}$. The potential vector is given by a sum of random phase modes as follows:

where $k = \sqrt{k_x^2 + k_y^2}$, $\phi \in [0, 2\pi)$ are random phases and $a(x)$ is a Gaussian-like convolution profile in the inhomogeneous direction going to zero at both boundaries and given by

$$a(x) = a_0 e^{-\left(\frac{x - x_{mp}}{2 L_{mp}}\right)^2} \tag{10}$$

where $x_{mp} = L_x/2 = 60$ and $L_{mp} = 1.66$ are the position and the thickness of our magnetopause model and a_0 a small amplitude such that the maximum absolute value of the initial perturbation is $\sim 10^{-3}$.

The simulation is run for about 1500 ion cyclotron times. Very rapidly, the initial perturbation reorganizes and sets up the reconnection eigenmodes that are identified by their wave-number in the y-periodic direction (each m wave-number is easily recovered by taking the Fourier Transform of the perturbation along the y-direction at a given time). Following the classical reconnection theory (Furth et al., 1963) (but ignoring the density inhomogeneity), we have checked that our equilibrium is Δ' unstable for the first five eigenmodes. We recall here that the Δ' parameter depends on the equilibrium magnetic shear and on the wavelength of the perturbation. It defines the instability threshold condition ($\Delta' \geq 0$). The unstable modes can be deduced by looking at Figure (4) where we plot Δ' as a function of the wave number m_y. We see that only the first five modes $m_y = 1, ..., 5$ correspond to a positive value of Δ', in agreement with the simulation where in the linear phase the $m_y \geq 6$ are stable (see discussion below). In Figure (5), panel (a), we plot the profile of the fastest growing eigenmode (corresponding to $m = 2$) of the x-component of the magnetic field fluctuation δb_x. The plot is along the inhomogeneous x-direction at five different times (see the legend) in log scale. The two red vertical dashed lines indicate the spatial window of the equilibrium represented in Figure (3). This picture shows that after an initial transient needed to set up the normal mode shape, the reconnection instability develops around the region where the magnetic field reverts, $0 \leq x \leq 16$ (see also Figure (3)). Since the equilibrium is asymmetric, in particular for what concerns the cold and hot ion density that vary in a different location with respect to the point where the magnetic field inverts, the eigenmode is not symmetric with respect to the point where the magnetic field inverts, $X_n \simeq 6.4$. To the best of our knowledge, this is the first time that one investigates the reconnection instability in the framework of a 3fluid approach in a non symmetric equilibrium representing directly the large-scale configuration taken from a satellite data event. Our goal here is to show the possibility to set up such a "realistic" large-scale initial equilibrium configuration to be simulated by a three-fluid approach. The non linear development of the system and in particular the mixing efficiency will be the object of future work. Still in Figure (5), panel (b), we plot the eigenmodes growth vs time in normalized units (log scale). We see the exponential growth of the first five modes, $m_y = 1, .., 5$. Modes with $m_y = 6, 7$ are instead stable. The orange curve corresponds to the most unstable mode, $m_y = 2$, the one plotted in
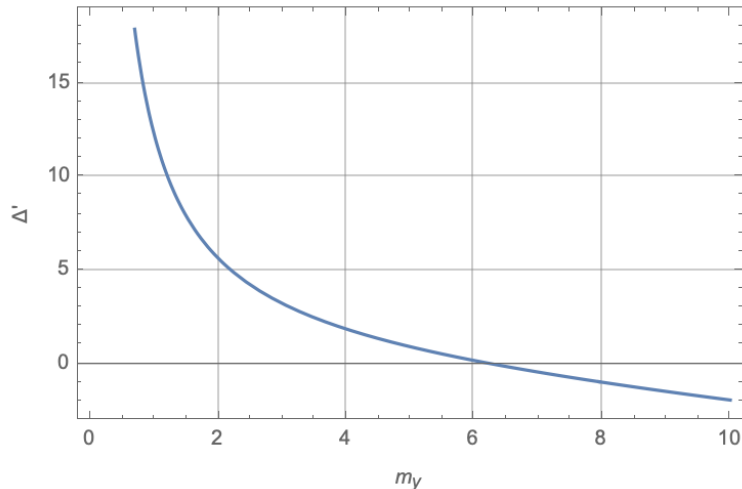
Figure 4. Δ' vs the wave number m_y for an equilibrium magnetic field $\sim tanh(x)$ (adimensional units). The unstable modes are those associated to positive values of Δ'.

315   panel (a). Despite the strong inhomogeneity of the system where, as discussed before, the magnetic inversion and the density variations occur at different locations, we see a very clear exponential growth with a constant growth rate. The linear phase last until about $t \simeq 1000$ after which the non linear phase begins. The value of the growth rate of the five unstable modes are reported in panel (c) confirming the theoretical trend shown in Figure 4. In particular $m_y = 2$ is the most unstable one. In Figure (6) we show at the beginning of the saturated phase, $t = 1455$ the shaded iso-contours of the cold ion population, $N_{i,c}$.

320   We see the formation of a hole structure corresponding to the region where the cold ion density grows eventually reaching the asymptotic magnetosheath value. To show the cold density hole, we made a cut along the inhomogeneous x-direction at $y = 38$ (see dashed line) still in Figure (6) in the bottom frame. In Figure (7) we show the same quantities for the hot ion fluctuations. We see a "complementary" behavior in the sense that now a bump is generated more or less in correspondence of the cold ion hole. However, as already discussed, it is not the goal of this paper to study the non linear dynamics and mixing properties of

325   the cold and hot ion populations. Our aim here is limited at presenting a method able to obtain a "realistic" 3fluid equilibrium starting from a set of satellite data that can be used as initial condition for the investigation of the dynamics in the framework of a three-fluid approach.

6   Conclusions

The huge amount of spacecraft data today available brings a lot of information about the magnetopause, especially those of

330   the MMS mission with their high resolution particle data. The magnetopause modeling can now be improved in view of these observations, which show that this boundary is never the simple textbook boundary generally considered. Beyond the natural asymmetry in temperature and density between the magnetosphere and magnetosheath plasmas, the first important ingredient
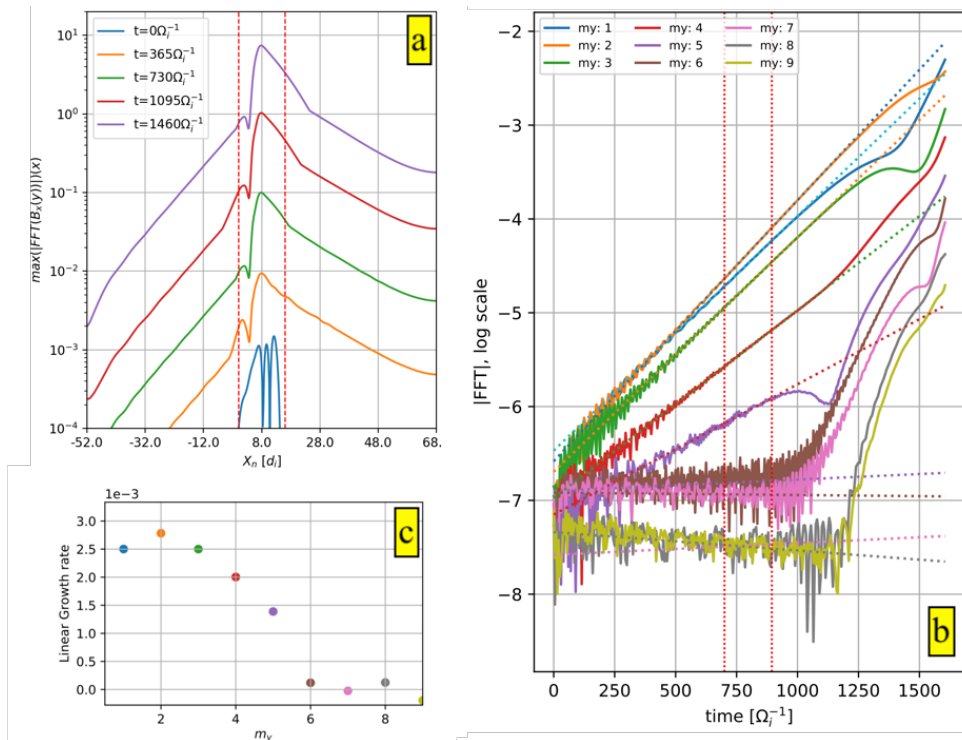
Figure 5. Development of the reconnection instability. Panel (a): the modulus of the Fourier Transform of δb_x along y vs x at five fixed time instant. The plots correspond to the fastest growing mode, $m = 2$, in log scale. The two red dashed vertical lines indicate the space interval of Figure (3). Panel (b): the first five eigenmodes growth vs time. The orange curve corresponds to the most unstable mode, $m = 2$, the one plotted in panel (a). Panel (c): the growth rate values vs k_y calculated by a best fit of the slopes in panel b. The colors correspond to those used in panel (b).

to consider is the strong velocity shear that arises at the boundary, in addition to the magnetic shear which is a defining property of the magnetopause. Furthermore, the gradients concerning the particles and those concerning the magnetic field

335 most generally have different locations and show different scale-lengths. The model has also to be able to be take into account these characteristics.

In this paper, we present for the first time a three-fluid equilibrium directly derived from data, using a magnetopause crossing by MMS. The derivation of the model is based on a fit of the experimental data for the most reliable ones, completed by a "realistic" solution of the equilibrium fluid equations for the others. The relative densities of the hot and cold ion popula-

340 tions calculated using the equilibrium equations provide an *a posteriori* check of our 3 fluid model. In particular, it helps understanding the different bulk quantities observed on the ion distribution functions (see panel (d) in Figure (1)).

Furthermore, a preliminary study shows that the model can be implemented in a three-fluid numerical simulation, validating the correctness of the equilibrium solution. The detailed study of the long time evolution of the magnetopause instability will be the subject for future work.
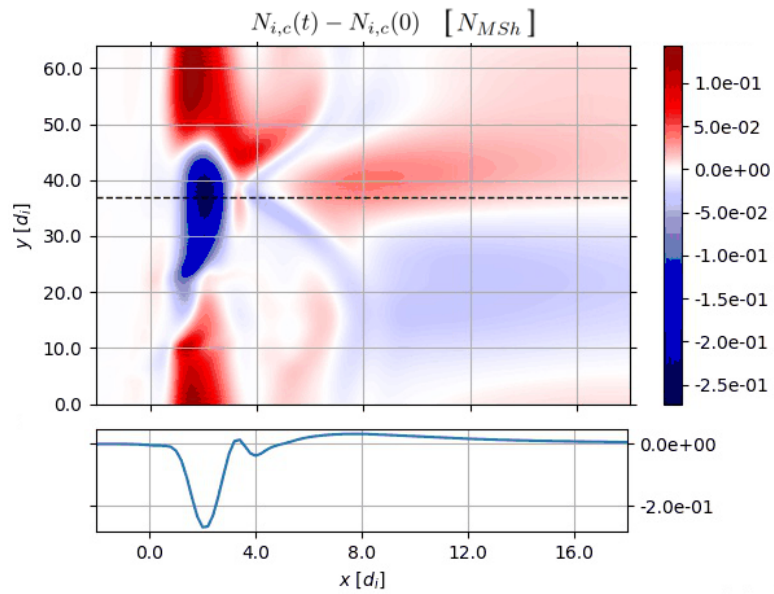
Figure 6. Shaded iso-contours of the cold ion fluctuations, $N_{i,c} - N_{i,c}(t=0)$ at $t = 1455\Omega_i^{-1}$. The bottom panel shows a plot of the same quantities vs x at $y \simeq 39$ corresponding to the horizontal dashed line in the shaded iso-contours. Numerical values are normalized to the magnetosheath density $N_{MSh} \sim 10cm^{-3}$.
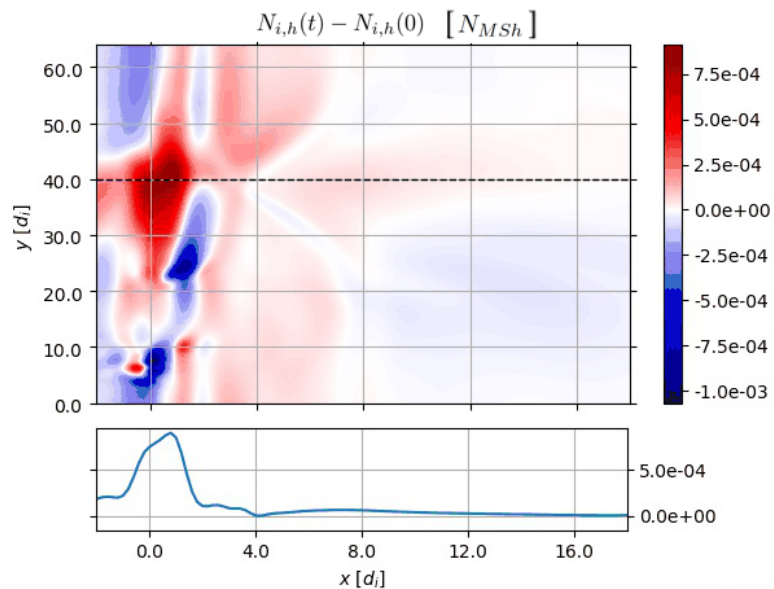
Figure 7. Same as Figure (6) for the hot ion fluctuations, $N_{i,h} - N_{i,h}(t=0)$.

345   It may seem contradictory to consider the data as characteristic of some magnetopause equilibrium and observe afterward that this equilibrium is not stable and should not last for long (even if the reconnection phenomenon is never "immediate"). To justify this point, one must understand that the main characteristics which are taken into account are the asymptotic values on each side, and in particular the velocity shear between magnetosheath and magnetosphere. These conditions are not changed by the instability. On the contrary, the positions and the scale of the different gradients can indeed be partly modified by the

350   instability. We think that this is one of the interesting issues that can be investigated by the time evolution observed in the simulation. How the system stability is impacted? (a parametric study is needed). How does it change in time due to non linear effects? Will the simulation converge toward a new more stable equilibrium state representative of the real system? All these points are the subject for future work.

Investigating the magnetopause stability and trying to understand, in particular, when and where reconnection phenomena

355   can be triggered and how the plasmas of both sides can get mixed, is still nowadays a challenging issue to be attacked by numerical simulations. However, knowing that the stability of a physical system is given by the specific initial equilibrium state, it must be kept in mind that the resulting non linear dynamics, in particular the mixing properties, also strongly depend on the choice of the initial equilibrium. As a consequence it is very important to initialize a simulation with a configuration as much realistic as possible. In most of the published literature, the simulations have been initialized with relatively simple

360   configurations, Harris sheets, or modified Harris sheets with little relationship with the real magnetopause. The realistic 3fluid equilibrium presented in this paper should therefore allow for a step further. The same method could be applied to other experimental cases in the future.

Data availability. All the data used are available on the MMS data server: https://lasp.colorado.edu/mms/sdc/public/about/browse-wrapper/.

Competing interests. The authors declare that no competing interests are present.

365   *Acknowledgements.* This project (FC) has received funding from the European Union's Horizon 2020 research and innovation program under grant agreement No 776262 (AIDA). The French involvement on MMS is supported by CNES and CNRS.

References

Alvarez Laguna, A., Mansour, N., Lani, A., and Poedts, S.: MULTI-FLUID MODELING OF THE EARTH'S MAGNETOSPHERE, in: Comparative Heliophysics Program, Summer 2016 at NASA Ames Research Center, https://lirias.kuleuven.be/retrieve/531033, 2016.

Aunai, N., Belmont, G., and Smets, R.: Proton acceleration in antiparallel collisionless magnetic reconnection: Kinetic mechanisms behind the fluid dynamics, Journal of Geophysical Research: Space Physics, 116, https://doi.org/10.1029/2011JA016688, 2011.

Baker, D. N. and Lanzerotti, L. J.: Resource Letter SW1: Space Weather, American Journal of Physics, 84, 166–180, https://doi.org/10.1119/1.4938403, 2016.

Belmont, G., Aunai, N., and Smets, R.: Kinetic equilibrium for an asymmetric tangential layer, Physics of Plasmas, 19, 022 108, https://doi.org/10.1063/1.3685707, 2012.

Bosqued, J. M., Phan, T. D., Dandouras, I., Escoubet, C. P., Rème, H., Balogh, A., Dunlop, M. W., Alcaydé, D., Amata, E., Bavassano-Cattaneo, M. B., Bruno, R., Carlson, C., Dilellis, A. M., Eliasson, L., Formisano, V., Kistler, L. M., Klecker, B., Korth, A., Kucharek, H., Lundin, R., McCarthy, M., McFadden, J. P., Möbius, E., Parks, G. K., and Sauvaud, J. A.: Cluster observations of the high-latitude magnetopause and cusp: initial results from the CIS ion instruments, Annales Geophysicae, 19, 1545–1566, https://doi.org/10.5194/angeo-19-1545-2001, 2001.

Büchner, J., Kuska, J.-P., and Wiechen, H.: Numerical Modelling and Simulation for Multi-Spacecraft Data Analysis: Approaches and Examples, ISSI Scientific Reports Series, 1, 449–478, 1998.

Burch, J. L., Torbert, R. B., Phan, T. D., Chen, L.-J., Moore, T. E., Ergun, R. E., Eastwood, J. P., Gershman, D. J., Cassak, P. A., Argall, M. R., Wang, S., Hesse, M., Pollock, C. J., Giles, B. L., Nakamura, R., Mauk, B. H., Fuselier, S. A., Russell, C. T., Strangeway, R. J., Drake, J. F., Shay, M. A., Khotyaintsev, Y. V., Lindqvist, P.-A., Marklund, G., Wilder, F. D., Young, D. T., Torkar, K., Goldstein, J., Dorelli, J. C., Avanov, L. A., Oka, M., Baker, D. N., Jaynes, A. N., Goodrich, K. A., Cohen, I. J., Turner, D. L., Fennell, J. F., Blake, J. B., Clemmons, J., Goldman, M., Newman, D., Petrinec, S. M., Trattner, K. J., Lavraud, B., Reiff, P. H., Baumjohann, W., Magnes, W., Steller, M., Lewis, W., Saito, Y., Coffey, V., and Chandler, M.: Electron-scale measurements of magnetic reconnection in space, Science, 352, aaf2939, https://doi.org/10.1126/science.aaf2939, 2016b.

Canuto, C.: Spectral methods in fluid dynamics, Springer series in computational physics, Springer-Verlag, ISBN: 9783540522058, https://www.springer.com/gp/book/9783540522058, 1988.

Channell, P. J.: Exact Vlasov–Maxwell equilibria with sheared magnetic fields, The Physics of Fluids, 19, 1541–1545, https://doi.org/10.1063/1.861357, 1976.

Chen, Y., Tóth, G., Cassak, P., Jia, X., Gombosi, T. I., Slavin, J. A., Markidis, S., Peng, I. B., Jordanova, V. K., and Henderson, M. G.: Global Three-Dimensional Simulation of Earth's Dayside Reconnection Using a Two-Way Coupled Magnetohydrodynamics With Embedded Particle-in-Cell Model: Initial Results, Journal of Geophysical Research (Space Physics), 122, 10,318–10,335, https://doi.org/10.1002/2017JA024186, 2017.

Cowley, S. W. H. and Owen, C. J.: A simple illustrative model of open flux tube motion over the dayside magnetopause, Planetary and Space Science, 37, 1461–1475, https://doi.org/10.1016/0032-0633(89)90116-5, 1989.

Dargent, J., Aunai, N., Lavraud, B., Toledo-Redondo, S., Shay, M. A., Cassak, P. A., and Malakit, K.: Kinetic simulation of asymmetric magnetic reconnection with cold ions, Journal of Geophysical Research: Space Physics, 122, 5290–5306, https://doi.org/10.1002/2016JA023831, 2017.

De Keyser, J. and Roth, M.: Equilibrium conditions and magnetic field rotation at the tangential discontinuity magnetopause, Journal of Geophysical Research: Space Physics, 103, 6653–6662, https://doi.org/10.1029/97JA03710, 1998.

Dorville, N., B. G., Aunai, N., D. J., and Rezeau, L.: Asymmetric kinetic equilibria: Generalization of the BAS model for rotating magnetic profile and non-zero electric field, Physics of Plasmas, 22, 092 904, https://doi.org/10.1063/1.4930210, 2015.

Dungey, J. W.: Interplanetary Magnetic Field and the Auroral Zones, Phys. Rev. Lett., 6, 47–48, https://doi.org/10.1103/PhysRevLett.6.47, 1961.

Fadanelli, S., Faganello, M., Califano, F., Cerri, S. S., Pegoraro, F., and Lavraud, B.: North-South Asymmetric Kelvin-Helmholtz Instability and Induced Reconnection at the Earth's Magnetospheric Flanks, Journal of Geophysical Research: Space Physics, 123, 9340–9356, https://doi.org/10.1029/2018JA025626, 2018.

Faganello, M. and Califano, F.: Magnetized Kelvin–Helmholtz instability: theory and simulations in the Earth's magnetosphere context, Journal of Plasma Physics, 83, 535830 601, https://doi.org/10.1017/S0022377817000770, 2017.

Faganello, M., Califano, F., and Pegoraro, F.: Being on time in magnetic reconnection, New Journal of Physics, 11, 063 008, https://doi.org/10.1088/1367-2630/11/6/063008, 2009.

Frey, H. U., Phan, T. D., Fuselier, S. A., and Mende, S. B.: Continuous magnetic reconnection at Earth's magnetopause, Nature, 426, 533–537, https://doi.org/10.1038/nature02084, 2003.

Furth, H. P., Killeen, J., and Rosenbluth, M. N.: Finite-Resistivity Instabilities of a Sheet Pinch, Physics of Fluids, 6, 459–484, https://doi.org/10.1063/1.1706761, 1963.

Hasegawa, H.: Structure and Dynamics of the Magnetopause and Its Boundary Layers, Monographs on Environment, Earth and Planets, 1, 71–119, https://doi.org/10.5047/meep.2012.00102.0071, 2012.

Labelle, J. and Treumann, R. A.: Plasma waves at the dayside magnetopause, Space Science Reviews, 47, 175–202, https://doi.org/10.1007/BF00223240, 1988.

Lee, L. C. and Roederer, J. G.: Solar wind energy transfer through the magnetopause of an open magnetosphere, Journal of Geophysical Research: Space Physics, 87, 1439–1444, https://doi.org/10.1029/JA087iA03p01439, 1982.

Lele, S. K.: Compact finite difference schemes with spectral-like resolution, Journal of Computational Physics, 103, 16 – 42, https://doi.org/10.1016/0021-9991(92)90324-R, 1992.

Ma, Y.-J., Nagy, A. F., Toth, G., Cravens, T. E., Russell, C. T., Gombosi, T. I., Wahlund, J.-E., Crary, F. J., Coates, A. J., Bertucci, C. L., and Neubauer, F. M.: 3D global multi-species Hall-MHD simulation of the Cassini T9 flyby, Geophysical Research Letters, 34, L24S10, https://doi.org/10.1029/2007GL031627, 2007.

Manuzzo, R., Belmont, G., Rezeau, L., Califano, F., and Denton, R. E.: Crossing of Plasma Structures by Spacecraft: A Path Calculator, Journal of Geophysical Research: Space Physics, n/a, https://doi.org/10.1029/2019JA026632, 2019.

Modolo, R., Chanteur, G. M., Dubinin, E., and Matthews, A. P.: Simulated solar wind plasma interaction with the Martian exosphere: influence of the solar EUV flux on the bow shock and the magnetic pile-up boundary, Annales Geophysicae, 24, 3403–3410, https://doi.org/10.5194/angeo-24-3403-2006, 2006.

Nakamura, M. and Scholer, M.: Structure of the magnetopause reconnection layer and of flux transfer events: Ion kinetic effects, Journal of Geophysical Research: Space Physics, 105, 23 179–23 191, https://doi.org/10.1029/2000JA900101, 2000.

Palmroth, M., Ganse, U., Pfau-Kempf, Y., Battarbee, M., Turc, L., Brito, T., Grandin, M., Hoilijoki, S., Sandroos, A., and von Alfthan, S.: Vlasov methods in space physics and astrophysics, Living Reviews in Computational Astrophysics, 4, 1, https://doi.org/10.1007/s41115-018-0003-2, https://doi.org/10.1007/s41115-018-0003-2, 2018.

Paschmann, G.: Observational Evidence for Transfer of Plasma Across the Magnetopause, Space Science Reviews, 80, 217–234, https://doi.org/10.1023/A:1004926004806, 1997.

Phan, T. D., Escoubet, C. P., Rezeau, L., Treumann, R. A., Vaivads, A., Paschmann, G., Fuselier, S. A., Attié, D., Rogers, B., and Sonnerup, B. U. Ö.: Magnetopause Processes, Space Science Reviews, 118, 367–424, https://doi.org/10.1007/s11214-005-3836-z, 2005.

445 Retinò, A., B. Bavassano-Cattaneo, M., Marcucci, M., Vaivads, A., André, M., Khotyaintsev, Y., Phan, T., Pallocchia, G., Rème, H., Möbius, E., Klecker, B., W. Carlson, C., McCarthy, M., Korth, A., Lundin, R., and Balogh, A.: Cluster multispacecraft observations at the high-latitude duskside magnetopause: Implications for continuous and component magnetic reconnection, Annales Geophysicae, 23, https://doi.org/10.5194/angeo-23-461-2005, 2005.

Roth, M., De Keyser, J., and Kuznetsova, M. M.: Vlasov theory of the equilibrium structure of tangential discontinuities in space plasmas,
450   Space Science Reviews, 76, 251–317, https://doi.org/10.1007/BF00197842, 1996.

Shi, Q. Q., Shen, C., Dunlop, M. W., Pu, Z. Y., Zong, Q.-G., Liu, Z. X., Lucek, E., and Balogh, A.: Motion of observed structures calculated from multi-point magnetic field measurements: Application to Cluster, Geophys. Res. Lett., 33, n/a–n/a, https://doi.org/10.1029/2005GL025073, l08109, 2006.

Shumlak, U., Lilly, R., Reddell, N., Sousa, E., and Srinivasan, B.: Advanced physics calculations using a multi-fluid plasma model, Computer
455   Physics Communications, 182, 1767–1770, https://doi.org/10.1016/j.cpc.2010.12.048, 2011.

Tanaka, K. G., Retinò, A., Asano, Y., Fujimoto, M., Shinohara, I., Vaivads, A., Khotyaintsev, Y., André, M., Bavassano-Cattaneo, M. B., Buchert, S. C., and Owen, C. J.: Effects on magnetic reconnection of a density asymmetry across the current sheet, Annales Geophysicae, 26, 2471–2483, https://doi.org/10.5194/angeo-26-2471-2008, 2008.

Whipple, E. C., Hill, J. R., and Nichols, J. D.: Magnetopause structure and the question of particle accessibility, Journal of Geophysical
460   Research: Space Physics, 89, 1508–1516, https://doi.org/10.1029/JA089iA03p01508, 1984.